




Article

Synthesis and Characterization of a Dysprosium(III)–Iron(III) Heterodinuclear Complex: Crystallographic, Hirshfeld Surface, Density-Functional Theory, and Luminescence Analyses

Mohd. Muddassir ^{1,*} , Abdullah Alarifi ¹, Naaser A. Y. Abduh ¹, Waseem Sharaf Saeed ² ,
Abdulnasser Mahmoud Karami ¹ and Mohd Afzal ¹ 

¹ Department of Chemistry, College of Science, King Saud University, Riyadh 11451, Saudi Arabia

² Restorative Dental Sciences Department, College of Dentistry, King Saud University, Riyadh 11545, Saudi Arabia

* Correspondence: muddassir@ksu.edu.sa

Abstract: Here, a new cyano-bridged 3d–4f compound, a Dy(III)–Fe(III) molecular assembly ([Dy(DMF)₄(H₂O)₃(μ-CN)Fe(CN)₅·H₂O] (1)), having a structure consisting of neutral one-dimensional (1D) chains, as well as an unbound aqua molecule, was synthesized and characterized using single crystal X-ray diffraction (XRD), infrared (IR), and elemental analyses. We then examined its structural topologies and studied its density functional theory (DFT), Hirshfeld surface analyses, and photophysical properties. The 1D chains were further linked by H-bond interactions, generating a three-dimensional (3D) motif which stabilizes the whole molecule. The weak interactions in **1** were assessed using Hirshfeld surface analyses, as well as fingerprint plots and DFT studies. Additionally, Hirshfeld surface analysis was performed to elucidate the roles of the weak interactions, such as the H···H, C···H, C–H···π, and van der Waals (vdW) interactions which are pivotal to stabilizing the crystal environment. Furthermore, the DFT studies were used to elucidate the bonding structure within the complex system. Complex **1** exhibits characteristic fluorescence as the Dy(III) complex is an excellent lime green luminescent material. Thus, it is considered to be a suitable material for preparing photoluminescent material.

Keywords: 3d–4f; one-dimensional Chain; Hirshfeld surface; DFT; hydrogen bonding; luminescence



Citation: Muddassir, M.; Alarifi, A.; Abduh, N.A.Y.; Saeed, W.S.; Karami, A.M.; Afzal, M. Synthesis and Characterization of a Dysprosium(III)–Iron(III) Heterodinuclear Complex: Crystallographic, Hirshfeld Surface, Density-Functional Theory, and Luminescence Analyses. *Crystals* **2022**, *12*, 1821. <https://doi.org/10.3390/cryst12121821>

Academic Editors: Ezzat Khan and Awal Noor

Received: 21 November 2022

Accepted: 12 December 2022

Published: 14 December 2022

Publisher's Note: MDPI stays neutral with regard to jurisdictional claims in published maps and institutional affiliations.



Copyright: © 2022 by the authors. Licensee MDPI, Basel, Switzerland. This article is an open access article distributed under the terms and conditions of the Creative Commons Attribution (CC BY) license (<https://creativecommons.org/licenses/by/4.0/>).

1. Introduction

The design and syntheses of cyano-bridged 3d–4f heterobimetallic molecular assemblies for the development of a wide range of functional materials have attracted tremendous interest over the past few decades [1–4]. The most frequently utilized homoleptic hexacyanometalates for these syntheses are [M(CN)₆]^{n−} compounds (where n = 2 or 3; and M = Fe, Co, Cr, V, or Mn) [5–7]. The luminescent properties of lanthanide(III)-based molecular assemblies have attracted substantial attention in the field of crystal engineering owing to their diverse topologies and intriguing structures [8–10], as well as their unique photophysical properties due to their 4fⁿ (n = 0–14) electronic configurations [8,11–13]. Lanthanide(III) ions exhibit large anisotropic magnetic moments and possess high coordination numbers and improved coordination flexibilities, which generally contribute to the production of outstanding metal building blocks in the presence of 3d transition metal hexacyanometalate ions such as [Fe(CN)₆]^{3−} and [Cr(CN)₆]^{3−} [5,9,14]. These ions are commonly employed as complex moieties to prepare the desired 3d–4f hybrid functional Prussian blue-like complexes via bottom-up self-assembly approaches, thus elucidating the structure–property relationship of the molecular framework [15,16].

Lanthanide (III) ions generally possess small molar absorption coefficients (this is due to their well-shielded 4f inner shells) which cause weak interactions between the

lanthanide ions, thereby generating weak luminescence [8]. The luminescent properties can be tuned by incorporating a bridging ligand, CN^- , between the lanthanide and transition metal centers to induce a metal-to-metal energy transfer process [17]. To date, reports relating to the investigation of the photophysical and electronic properties of cyano-bridged 3d–4f complexes are limited [12,18–21]. Most reports are focused on their magnetic properties [1,5,7,9,22]. Moreover, due to the interaction between the cyanometalate and transition metal centers, the electrostatic crystal field influences the energy levels of the d-orbitals and generates different crystal structures [23]. These complexes exhibit different bands in the visible region, and are consequently assumed to be promising optical and photomagnetic materials whose electronic states can be adjusted using visible light [4,16,24]. Moreover, several intrinsic characteristics, such as the luminescence quantum yield (QY), narrow emission bands, and long emission lifetimes, make it interesting to explore the unusual photophysical features of the molecular framework [10,25].

The different coordination numbers of lanthanide (III) ions allow their coordination with solvent molecules to generate polymeric complexes of different dimensions [26]. Further, exclusion of solvent molecules can cause the breakdown of the polymeric networks [5]. In this context, several frameworks of varying dimensionalities which were obtained from hexacyanometalates and lanthanide ions have been investigated, and their stabilities and dimensionalities have been controlled by a solvent molecule (N,N-dimethylformamide) and a heterocyclic moiety as a blocking ligand with various stages of hydration [3,14,27,28]. Recently, Chorazy et al. studied the photoluminescence properties of a cyanido-bridged, layered Dy(III)–Co(III) material by examining the yellow to greenish blue color as tunable photoluminescence at selected wavelengths [29].

Based on the above, and in furtherance of our ongoing research to develop new cyano-based complexes [30–33], this work presents the synthesis, structural topologies, density-functional theory (DFT), and photophysical properties of a cyanide-bridged Dy(III)–Fe(III) molecular assembly, which was identified as $[\text{Dy}(\text{DMF})_4(\text{H}_2\text{O})_3(\mu\text{-CN})\text{Fe}(\text{CN})_5\cdot\text{H}_2\text{O}]$ (**1**). The structures of **1** were confirmed by its single crystal X-ray diffraction (XRD) patterns and other analytical and spectroscopic measurements.

2. Experimental Section

2.1. Starting Materials

All of the starting materials, including the solvents, were purchased from commercial sources as analytical reagents and utilized without further purification. The ultraviolet–visible (UV–Vis) solid state spectrum of the dried sample was measured using a Shimadzu UV-3600 spectrometer (Kyoto, Japan). The photoluminescence spectra were obtained from the solid films, which were prepared by drop-casting an N,N-dimethylformamide (DMF) suspension of **1** onto a quartz plate and employing a Nanolog spectrofluorometer from HORIBA Jobin Yvon. Thermogravimetric analysis with differential scanning calorimetry (TGA/DSC) was performed in a nitrogen atmosphere utilizing alumina powder as the reference material using a Universal V3.8B TA SDT Q600 Build 51 thermal analyzer (TA Instruments, New Castle, DE, USA).

Caution! Cyanides are hypertoxic and hazardous and should be handled in small quantities with great caution!

2.2. Synthesis

A solution of $\text{Dy}(\text{NO}_3)_3\cdot 6\text{H}_2\text{O}$ (43.8 mg, 0.1 mmol) was first dissolved in methanol (MeOH, 6 mL), followed by the dropwise addition of $\text{K}_3[\text{Fe}(\text{CN})_6]$ (32.9 mg, 0.1 mmol) in H_2O (4 mL) with continuous stirring. The yellow precipitate obtained was dissolved in DMF (4 mL). The resulting mixture was allowed to stand undisturbed in the dark for one week, after which yellow block-shaped single crystals of **1** were obtained, which were suitable for X-ray analysis (yield = 41%). The result of the elemental analysis of $\text{C}_{18}\text{H}_{36}\text{DyFeN}_{10}\text{O}_8$ was as follows: Calculated: C, 29.26; H, 4.91; N, 18.96%. Found: C, 28.97; H, 4.79; N, 18.81%.

The X-ray crystal structure determination, topological description, and computational methodology are presented in detail in the supporting information (See the Supplementary Materials).

3. Results and Discussion

3.1. Investigation of the X-ray Structure

The molecular structures of the synthesized complex were confirmed by single crystal X-ray structure analysis. For the single crystal XRD analysis of complex **1**, suitable crystals were obtained from the slow evaporation of a MeOH:DMF (3:1) solution. The structure of **1** is shown in Figure 1a, and the crystallographic data are listed in Table 1. Further, the bond distances and angles are presented in Table 2. The details of the data collection and refinement are presented in the experimental section. The structure was solved by a monoclinic system containing a $P2_1/c$ space group, and the structure consisted of neutral one-dimensional (1D) chains, in addition to an unbound aqua molecule. Only one aqua molecule, in addition to a hydrogen-bonded water molecule, was present in the asymmetric unit. The molecular structure consisted of a cyano-bridge array of $\text{Fe}(\text{CN})_6$ and $\text{Dy}(\text{DMF})_4(\text{H}_2\text{O})_3$ fragments, which formed heterobimetallic molecular entities that were linked by a CN^- -bridged ligand. Dy(III) is eight-coordinated, with a distorted square antiprism geometry. Seven oxygen atoms were found to surround Dy^{+3} : three water and four DMF molecules. Additionally, one H_2O ligand was connected to the uncoordinated H_2O molecule via H-bonds. Furthermore, the nitrogen atoms of the bridging CN^- ligand occupied the eighth coordination position. The distance of the Dy–O bond ranged between 2.342(3) and 2.401(3) Å. The distinction in the distances between the Dy–O bonds and the DMF and water groups was evident (on average, the Dy–O bonds of the latter were longer by ~ 0.02 Å and the longest Dy(III)–ligand distance corresponded to the nitrogen atom of the CN^- bridge (2.421(3)). Further, Fe(III) was surrounded by six cyanide ligands in a distorted octahedral environment, and the Fe–C distances ranged from 1.931 to 1.945 Å. The intramolecular distance between the two metals through the CN^- bridge was $\text{Dy}\cdots\text{Fe} = 5.439$ Å. The neutral dinuclear units were linked by H-bonds in a three-dimensional (3D) network. The 3D network altered the [Dy–Fe] dinuclear entities that were linked by H-bonds between the five terminal CN^- groups of the $\text{Fe}(\text{CN})_6$ fragment, the three oxygen atoms of the H_2O ligand in the $\text{Dy}(\text{DMF})_4(\text{H}_2\text{O})_3$ fragment, and the water molecules of crystallization. Dy(III) exhibits a coordination number (8) and a square antiprismatic geometry, as shown in Figure S1, and has been further analyzed using the SHAPE program [34] to reveal the same geometry, as summarized in Table 3, which also shows the distorted square antiprism (SAPR–8) of Dy(III).

The structure can be simplified into its underlying net in a so-called standard representation, in which all the metal atoms and centers of mass of ligands are nodes of the underlying net [35]. Such a representation indicated that the structure consisted of molecular monohydrate complexes that formed a 5-nodal 1, 1, 2, 6, 8-c net, with a $(1-c)7(1-c)5(2-c)(6-c)(8-c)$ stoichiometry of the 1, 1, 2, 6, 8M15-1 topological type (Figure 1b).

The H-bonds with uncoordinated H_2O were not the only non-valence bonds within the structure. As previously described, the molecular complexes were connected by hydrogen bonds either directly or through the bridging H_2O molecules. This necessitated further analyses to consider hydrogen bonding. In this approach, the binuclear complexes and H_2O bridges, which were considered as the net nodes, were connected by hydrogen bonds. The representation of the H-bonded standard obtained a 3, 7-c 2-nodal underlying net (Figure 1c,d). This net was two-dimensional; the layers were parallel to the (1,0,0) planes. The determined topology type (3, 7L55) occurred three times among all of the known structures in the standard representations of the H-bonded or specific-bonded molecular structures, and once in the standard representations of the Coulomb- or vdW-bonded molecular structures [36–38].

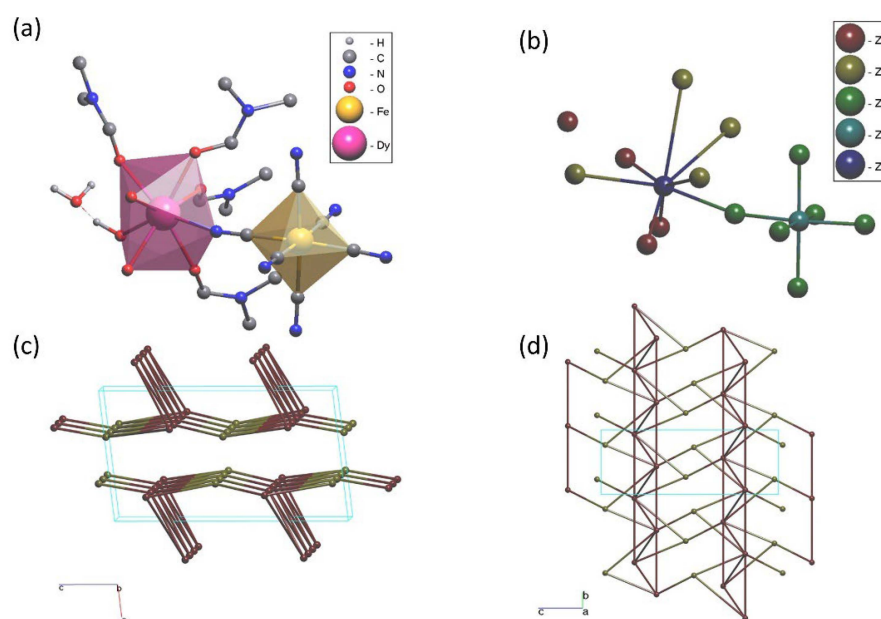


Figure 1. (a) Molecular complex with a $C_{18}H_{36}DyFeN_{10}O_8$ composition. (b) Standard representation of the underlying net (right). ZA = H_2O , ZB = DMF, ZC = CN, ZD = Fe, ZE = Dy. The hydrogen atoms that did not participate in the H-bonding were omitted for clarity. The underlying net in the standard representation of the H-bonded molecular metal–organic frameworks (MOFs) is shown in the (c) (0,1,0) (left) and (d) (1,0,0) projections. The red spheres represent the molecular complexes; the yellow spheres describe the H_2O molecules. The unit cell of the structure is represented by a blue line.

Table 1. Crystal data and structure refinement for 1.

CCDC Number	2035107
Empirical formula	$C_{18}H_{36}DyFeN_{10}O_8$
Formula weight	738.92
Temperature/K	100(2)
Crystal system	monoclinic
Space group	$P2_1/c$
a/Å	13.8891(12)
b/Å	8.8619(8)
c/Å	24.681(2)
$\alpha/^\circ$	90
$\beta/^\circ$	96.7250(10)
$\gamma/^\circ$	90
Volume/Å ³	3016.9(5)
Z	4
$\rho_{\text{calc}}/\text{cm}^3$	1.627
μ/mm^{-1}	2.993
F(000)	1480.0
Crystal size/mm ³	$0.230 \times 0.160 \times 0.110$
Radiation	MoK α ($\lambda = 0.71073$)
2 θ range for data collection/ $^\circ$	2.952–50.1
Index ranges	$-16 \leq h \leq 16, -8 \leq k \leq 10, -29 \leq l \leq 16$
Acquired reflections	16022
Independent reflections	5335 [$R_{\text{int}} = 0.0261, R_{\text{sigma}} = 0.0280$]
Data/restraints/parameters	5335/0/354
Goodness-of-fit on F^2	1.146
Final R indexes [$I \geq 2\sigma(I)$]	$R_1 = 0.0310, wR_2 = 0.0733$
Final R indexes [all the data]	$R_1 = 0.0317, wR_2 = 0.0738$
Largest diff. peak/hole/eÅ ^{−3}	1.93/−1.07

Table 2. Selected bond distances (Å) for **1**.

	Complex 1	
	X-ray	DFT
Dy1–O1	2.384(3)	2.451
Dy1–O2	2.369(3)	2.453
Dy1–O3	2.342(3)	2.437
Dy1–O4	2.357(3)	2.389
Dy1–O5	2.401(3)	2.541
Dy1–O6	2.372(3)	2.398
Dy1–O7	2.347(3)	2.441
Dy1–N5	2.421(3)	2.523
Fe1–C1	1.951(4)	2.204
Fe1–C2	1.940(4)	2.183
Fe1–C3	1.936(4)	2.012
Fe1–C4	1.945(4)	2.013
Fe1–C5	1.943(4)	2.522
Fe1–C6	1.931(4)	2.097

Table 3. SHAPE analyses of Dy(III) in **1**.

Structure			
[Dy(III)]	(SAPR-8) ^a	(DD-8) ^a	(BTP-8) ^a
1	0.797448	1.476427	4.732264

^a SAPR-8: D_{4d} , square antiprism; DD-8: D_{2d} , triangular dodecahedron; BTP-8: D_{3d} , bicapped trigonal prism.

The standard representation of the vdW-bonded molecular structures is as a 3D framework. The unique 6,22-c 2-nodal net obtained (Figure 2a) exhibited an unknown topology with a point symbol, $\{3^{13}.4^2\}\{3^{71}.4^{133}.5^{27}\}$. Conversely, the uncoordinated H_2O molecules were much smaller than the complexes, thus barely affecting the packing. Therefore, the underlying net without consideration of uncoordinated H_2O , which also exhibited an unknown topology, was a 16-c uninodal net (Figure 2b) with the point symbol $\{3^{45}.4^{66}.5^9\}$.

The DFT method was selected as an alternative way to validate the molecular structure of **1**. The geometrical optimization of **1** was performed without symmetry restrictions on the compounds, and the optimized structures are shown in Figure 2c. The structural parameters of the final structures are in good agreement with those obtained by XRD for similar systems (Table 1).

3.2. IR Spectroscopy

In **1**, a broad band around 3415 cm^{-1} indicated the presence of a water molecule, as shown in Figure 2d. The stretching frequencies of the C=O bonds, which correspond to the coordinated DMF molecule, are located at $\sim 1635\text{ cm}^{-1}$ [30]. The terminal cyano ligands of $[Fe(III)(CN)_6]$ exhibited sharp $C\equiv N$ stretching bands at $\sim 2096\text{ cm}^{-1}$; whereas in the bridging CN^- ligands, the stretching bands generally shifted to higher frequencies because of the depletion of the electron density in the weakly antibonding 5σ orbital of the CN^- ligand. However, in **1**, the IR spectra exhibited pronounced $C\equiv N$ stretching bands at lower frequencies than those of the $[Fe(III)(CN)_6]$ moiety. Complex **1** displayed two peaks at 2144 (strong) and 2065 (weak) cm^{-1} , which exhibited the presence of two or more nonequivalent CN^- species in the complex, such as the bridging and terminal modes. This also agrees with the single crystal X-ray structure [39]. Furthermore, the formation of the heterometallic complex was revealed by the presence of medium intensity (Dy–O) bands in the far-IR region, at approximately 420 cm^{-1} . The IR spectra also indicated that the +3 oxidation state of iron [40] was maintained in the complex.

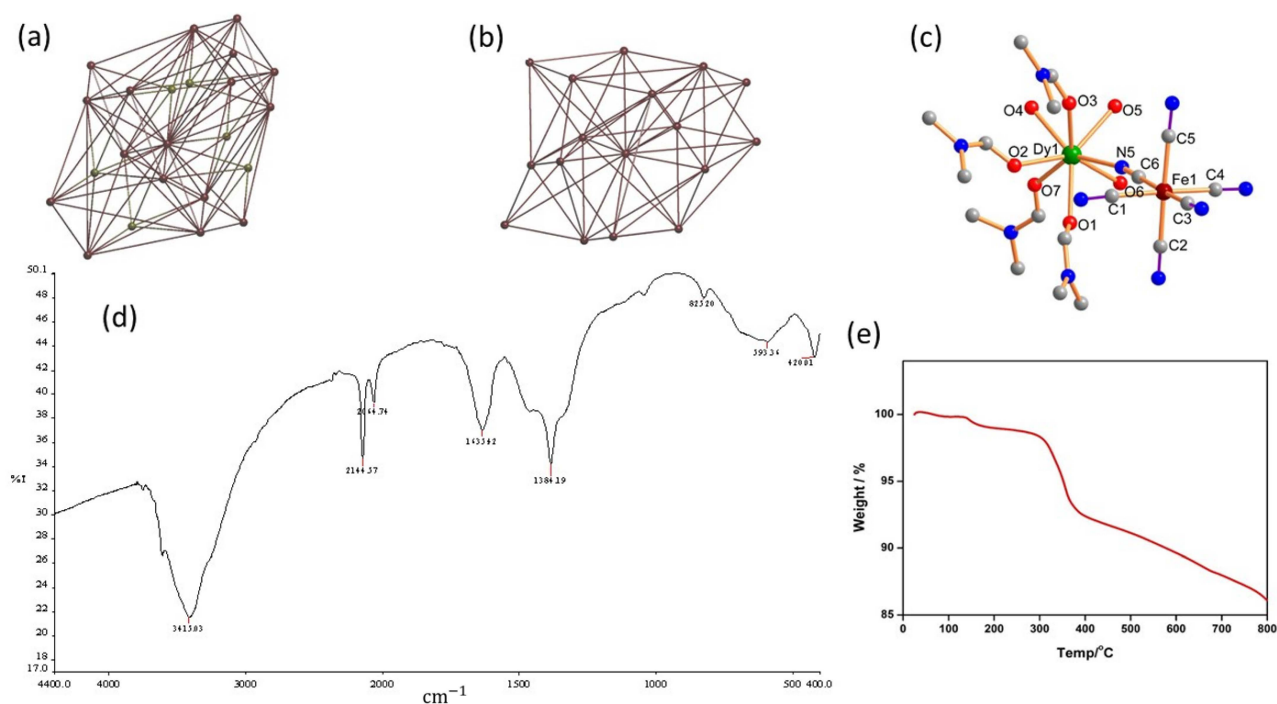


Figure 2. (a,b) Underlying net in the standard representation of the Coulomb- or vdW-bonded molecular structures, when considering the uncoordinated H₂O (left) or not (right). The red spheres describe the molecular complexes; the yellow spheres describe the H₂O molecules. (c) DFT-optimized structures of **1**. H-atoms and H₂O were omitted for clarity. (d) IR spectrum of **1**. (e) TGA spectrum of **1**.

3.3. TGA

TGA of **1** was performed to study the weight-loss pattern in the temperature range of 25–800 °C, as shown in Figure 2e; it was found that the weight loss occurred in two steps. The noticeable weight loss in the temperature range of 100–385 °C indicated the removal of the four water molecules (observed weight loss = 7.9%; calculated = 9.7%), thereby indicating that **1** exhibited high thermal stability. Subsequently, **1** began to decompose around 400 °C; this is consistent with the results of other similar complexes [30].

3.4. Mass Spectrometry (MS)

The complex was unambiguously characterized by MS analysis. The electrospray mass spectra of the copper complex revealed the molecular ion peaks, and also exhibited other peaks which were due to the successive fragmentation of the complex, as shown in Figure S2. The mass spectrum of **1** exhibited molecular ion peaks at 480, which correspond to $[(\text{Dy}(\text{DMF})_4(\text{H}_2\text{O})_3(\mu\text{-CN})\text{Fe}(\text{CN})_5\cdot\text{H}_2\text{O})-3\text{DMF}\cdot 2\text{H}_2\text{O} + 4\text{H}^+)]^+$, caused by the removal of labile DMF and the aqua molecules.

3.5. Powder XRD (PXRD)

Meanwhile, the PXRD data of Complex **1** matched well with that simulated from the single crystal data, which demonstrated that the bulk samples have the same structure as the single crystal X-ray sample, proving the phase purity; as also shown via ESI, Figure S3.

3.6. Analysis of the Frontier Molecular Orbitals (FMO)

Frontier molecular orbitals (FMOs), i.e., the highest occupied MOs (HOMOs), and the lowest unoccupied MOs (LUMOs), are pivotal in demonstrating the chemical reactivity, kinetic stability, and electrical transport properties of a molecule. The low degree of intramolecular charge transfer (ICT) from the electron-donating groups to the electron-accepting ones correlated with a small HOMO–LUMO gap. A large HOMO–LUMO energy gap indicates that molecules are highly stable, as demonstrated by their lowered reactions

to chemical and biochemical responses. Molecular systems with a high energy of HOMO (E_{HOMO}) are good electron donors, whereas those with low E_{LUMO} are good electron acceptors. The calculated energy gap between HOMO and LUMO for **1** was -1.83 eV. Furthermore, a major part of the LUMOs was centered on the coordinated DMF moieties, while the HOMOs were mainly localized on the Fe^{+3} and the CN^- ligand (Figure 3).

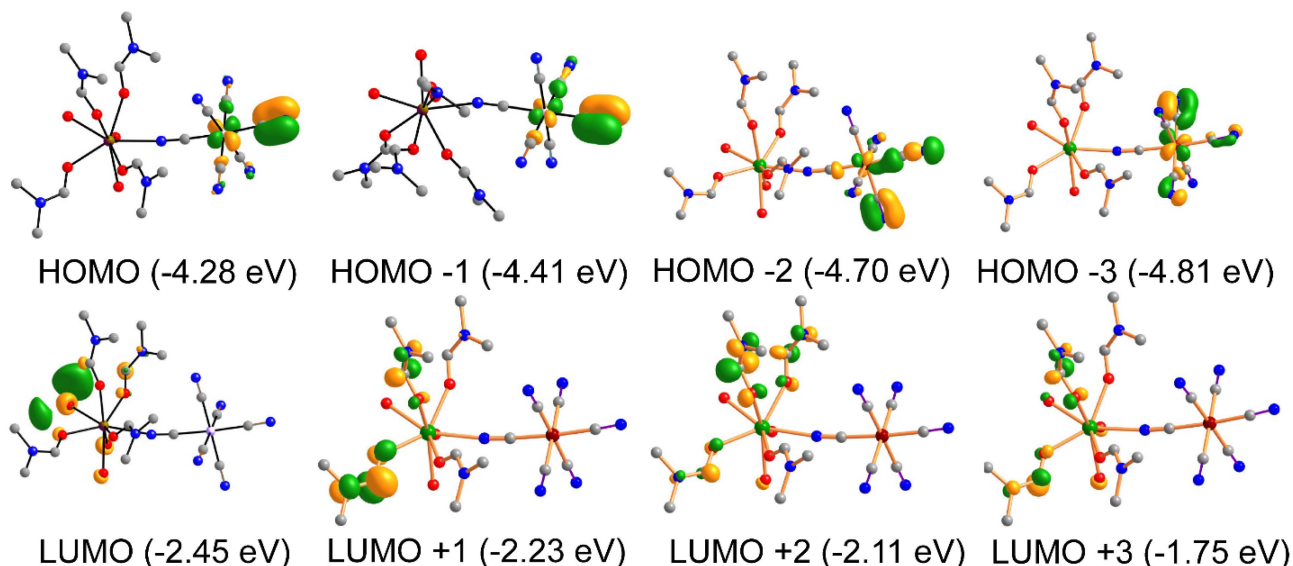


Figure 3. FMO involved in the electronic transitions that were observed in time-dependent DFT (TDDFT)-calculated UV–Vis spectrum of **1**.

3.7. Hirshfeld Surface Analyses

CrystalExplorer is an essential tool for examining the structures of crystals; it visualizes the interactions within crystal structures through the Hirshfeld surface and fingerprint plots [41]. The Hirshfeld surface was mapped by d_{norm} (normalized interaction distance), which was normalized from d_e (the nearest external distance), d_i (the nearest internal distance), and the van der Waals (vdW) radii from the atoms to the surface [42]. The surface area was the same as the one obtained from d_e (the nearest external distance). The fingerprint plots were obtained from the 3D Hirshfeld surface, which avails a visual overview of the frequency of any combination of d_e and d_i on the surface of a molecule. Thus, they exposed the intermolecular interactions that were present, and depicted the details of the relative surface area of each interaction.

The Hirshfeld surfaces of **1** are shown in Figure 4 and represent the surfaces that were plotted around a d_{norm} range of -0.53 to 1.28 Å, a shape index of -1.0 to 1.0 Å, and a curvedness of -4.0 to 4.0 Å. The d_{norm} factor is exhibited as a red–white–blue surface color scheme, while the deep red-colored spots depict shorter contacts, e.g., H-bonding. The white zones denote the vdW interactions for separations such as the $H \cdots H$ contacts, and the blue regions are those that are devoid of close contacts. The red regions, which correspond to $C-H \cdots \pi$ interactions, and the ‘bow-tie patterns’, which indicate the presence of aromatic stacking ($\pi \cdots \pi$) interactions, can be examined on the Hirshfeld surface that was mapped with a shape index function [43]. The curvedness of the surface corresponds to the electronic densities of the curved surface around the molecular contacts. In the d_{norm} surface of **1**, the prevalence of the blue and white surfaces over the red ones indicates that the hydrophobic interaction due to the aromatic ring was dominant. The dark red- and blue-colored spots are distributions in the shape index of the surface that correspond to the $C-H \cdots \pi$ interactions in **1**.

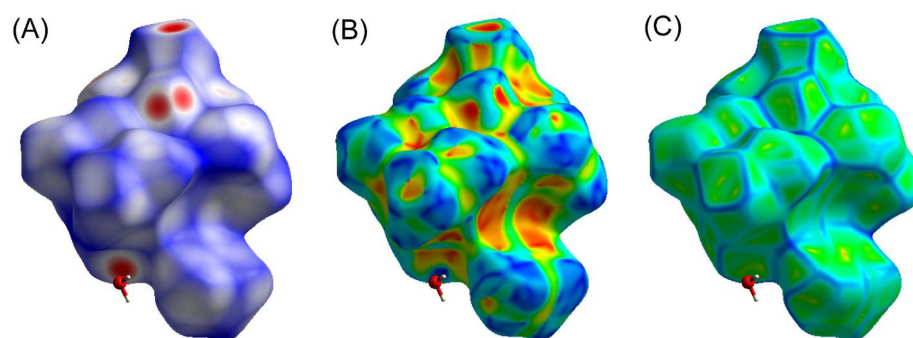


Figure 4. Hirshfeld surfaces of **1** mapped with d_{norm} (A), shape index (B), and curvedness (C).

Figure 5 displays the fingerprint plots, split into atom pair close contacts. This analysis permits the distinction of contributions from different interactions, which overlap in the full fingerprint. For **1**, the proportions of the $\text{H} \cdots \text{H}$, $\text{O} \cdots \text{H}$, $\text{C} \cdots \text{H}$, and $\text{N} \cdots \text{H}$ interactions comprised 39.50%, 7.20%, 15.40%, 10.20%, and 37.10% of the total Hirshfeld surface of each molecule, respectively.

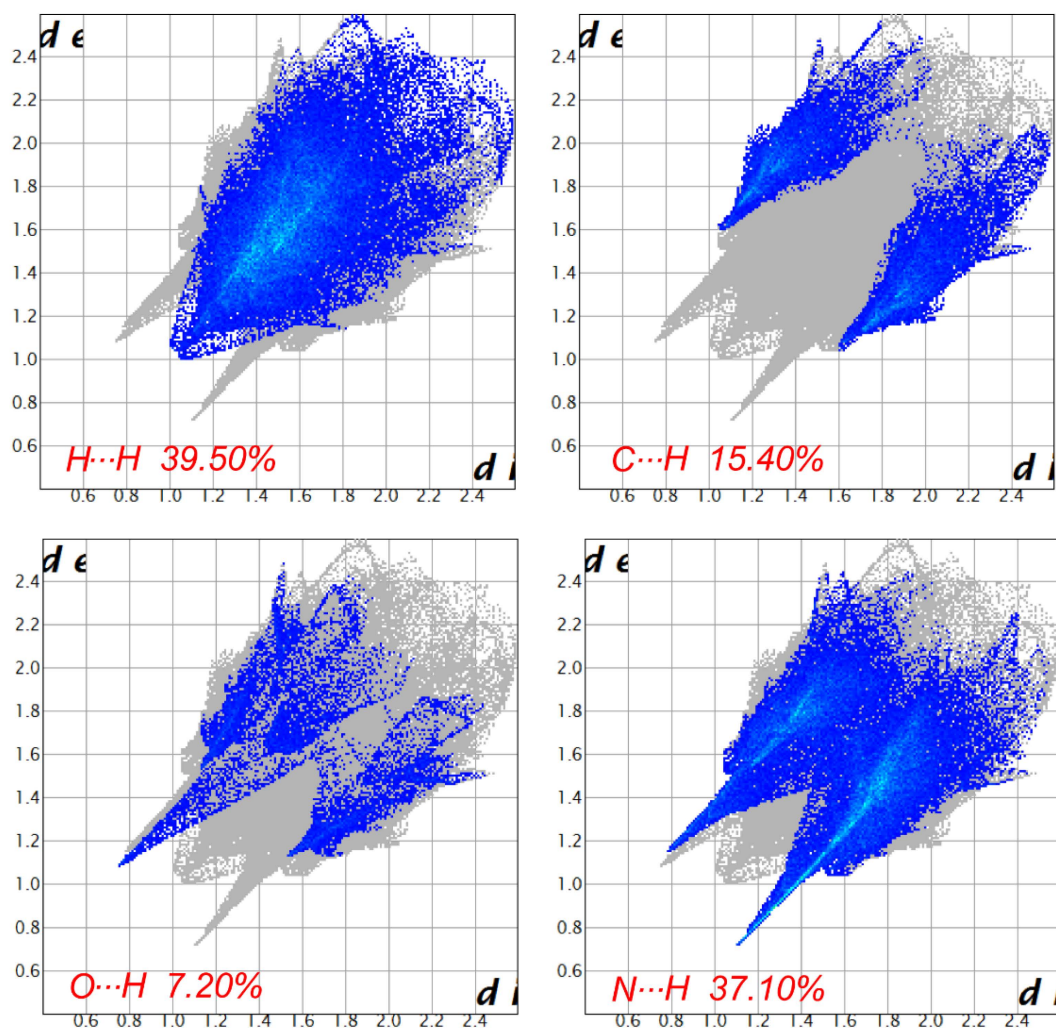


Figure 5. Two-dimensional fingerprint plots of the interatomic interactions of **1** displaying the percentages of the contacts that contributed to the total Hirshfeld surface area of the molecules.

3.8. Absorption Spectrum

The effect of the interaction between Dy(III) and Fe(III) ions through cyano-bridges resulted in a different charge distribution, i.e., the decreasing extent of π back-donation. As elucidated by these results, this effect, which is a combination of structural and electronic factors, was observed for specific Dy(III) elements that were remarkable for the ground states of the complex. The UV–Vis absorption spectra of the Dy(III)–Fe(III) complex system investigated was carried out in a DMF solvent in the range of 220–700 nm at room temperature (Figure 6a). There were two major absorption peaks at 266 and 310 nm, followed by a shoulder, which was due to the π – π^* transitions of the DMF ligand and low-spin $[\text{Fe}(\text{CN})_6]_3$. It was evident that the coordination bonds of the $[\text{Fe}(\text{CN})_6]_3$ moiety were via π back-donation, in which five $3d$ electrons that occupied the t_{2g} orbitals were donated to the unoccupied π^* orbitals of the cyanide ligands. In the case of the O_h symmetry, the $3d$ electron configuration of Fe(III) was $t_{2g}^5 e_g^0$, and the configurations of the $2p$ orbitals of the cyanide ligands were t_{1g} , t_{1u} , t_{2g} , and t_{2u} . Following the excitation of the cyanide electrons to the π^* orbitals (formed from the unoccupied t_{1g} , t_{1u} , and t_{2u} orbitals), which were associated with metal-to-ligand CT (MLCT) from the t_{2g}^5 orbital in Fe(III) to the unoccupied π^* orbitals in the cyanide ligands, the π back-donation was probably weakened by t electronic repulsion in the unoccupied π^* orbitals. In the Vis region, the spectrum was dominated by two low energy bands that were centered at 430 and 575 nm, which corresponded to the $^4F_{9/2} \rightarrow ^6H_{15/2, 13/2}$ transitions that were responsible for the lime green emission of these molecules. The absorption bands that were due to the f – f transitions of Dy(III) became weak as they were obscured by the strong transition of the ligand.

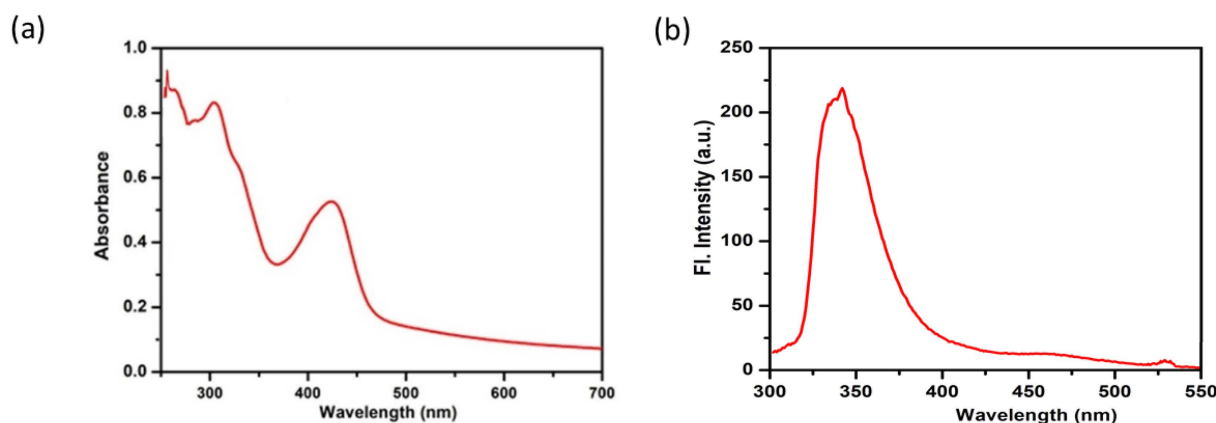


Figure 6. (a) UV–Vis absorption and (b) luminescence spectra of **1** at room temperature ($\lambda_{\text{ex}} = 300$ nm).

3.9. Steady-State Luminescence Study

The luminescent properties of lanthanide complexes are of great interest, owing to their unique light emission which originates from their $4f$ core-like orbitals [2,44–46]. In particular, a cyanide-bridged heterobimetallic system is an attractive candidate for the harnessing of photoluminescent properties, since the short inorganic CN^- linkage can strongly couple with two metal centers, thus inducing efficient metal-to-metal and metal-to-ligand CT (MLCT) processes. Dy(III)-based luminescent materials have been reported to exhibit strong luminescence [18]. However, the luminescent properties of cyanide-bridged Dy(III)–Fe(III) heterobimetallic systems have scarcely been studied. Upon excitation at 300 nm at room temperature, the fluorescence spectrum of **1** exhibited one characteristically structured intense emission band at 343, and two weak bands at 465 and 540 nm (Figure 6b). The sharp emission band at 343 nm was ascribed to the intramolecular energy transfer from the ligand to the emitting energy state of Dy(III) [47]. However, the weak emission bands at 460 and 530 nm correspond to the $^4F_{9/2} \rightarrow ^6H_{15/2}$ and $^4F_{9/2} \rightarrow ^6H_{13/2}$ transitions of the $4f$ electrons of Dy(III), respectively [47]. Thus, it was inferred that the appearances of the weak characteristic emissions of Dy(III) and Fe(III), and the fluorescence of the ligand,

might be due to the competition between the fluorescence of the ligand and the energy-transfer process from the lowest triplet state of the ligand to the excited states of Dy(III) and Fe(III), which are responsible for the apparent lime green emission of this system. Complex **1** exhibited characteristic fluorescence, thereby presenting the Dy(III) complex as an excellent lime green luminescent material that could be considered for applications in organic light-emitting devices (OLEDs) and medical diagnostics.

4. Conclusions

A new 1D complex, **1**, was synthesized and structurally characterized to form alternating bridging cyanide ligands, i.e., the compounds consisted of 1D chains in which Dy(III) and Fe(III) were linked in an alternating fashion. These chains were further linked by H-bond interactions, which generated a 3D motif that stabilized the molecule. These interactions were validated by Hirshfeld surface analysis. In **1**, the H \cdots H, O \cdots H, C \cdots H, and N \cdots H interactions comprised 39.50%, 7.20%, 15.40%, 10.20%, and 37.10% of the total Hirshfeld surface of each molecule, respectively. Owing to the availability of a significant number of hydrogen atoms in the compound, and because of the non-planarity of the molecular geometry, several hydrogen atoms were at distances that were less than the sum of their vdW radii. Thus, they actively contributed to the stability of the supramolecular architecture, and consequently stabilized the molecule. Further computational studies (DFT) supported the experimental observations. The excellent luminescence property of the complex avails it as a suitable material for constructing photoluminescent materials for exploring intrinsic optical properties. The reported complex, and similar complexes, are suitable materials for constructing magnetic materials whose uses, such as for quantum computing and information storage, could be further studied. We anticipate further research on these types of materials for the development of advanced multifunctional materials.

Supplementary Materials: The following supporting information can be downloaded at: <https://www.mdpi.com/article/10.3390/cryst12121821/s1>, Figure S1: Schematic representation of the distorted square antiprism coordination environment of the Dy(III) metallic center in $[\text{Dy}(\text{DMF})_4(\text{H}_2\text{O})_3(\mu\text{-CN})\text{Fe}(\text{CN})_5\cdot\text{H}_2\text{O}]$ (**1**); Figure S2: Mass spectrum of complex **1**; Figure S3: Powder XRD patterns of simulated (blue, up) from the single-crystal data and powder XRD patterns of experimental (red, down) of the complex **1**.

Author Contributions: Methodology, A.A.; Formal analysis, N.A.Y.A.; Data curation, M.M. and A.M.K.; Writing—original draft, M.M. and M.A.; Writing—review and editing, W.S.S.; Project administration, M.M. All authors have read and agreed to the published version of the manuscript.

Funding: This research received no external funding.

Acknowledgments: The authors extend their appreciation to the Deputyship for Research & Innovation, Ministry of Education in Saudi Arabia for funding this research work through the project number IFKSURG-2-1502.

Conflicts of Interest: The authors declare no conflict of interest.

References

1. Figuerola, A.; Diaz, C.; Ribas, J.; Tangoulis, V.; Granell, J.; Lloret, F.; Mahía, J.; Maestro, M. Synthesis and characterization of heterodinuclear Ln^{3+} – Fe^{3+} and Ln^{3+} – Co^{3+} complexes, bridged by cyanide ligand (Ln^{3+} = Lanthanide Ions). Nature of the magnetic interaction in the Ln^{3+} – Fe^{3+} complexes. *Inorg. Chem.* **2003**, *42*, 641. [CrossRef] [PubMed]
2. de Sá, G.; Malta, O.; Donegá, C.D.M.; Simas, A.; Longo, R.; Santa-Cruz, P.; da Silva, E. Spectroscopic properties and design of highly luminescent lanthanide coordination complexes. *Coord. Chem. Rev.* **2000**, *196*, 165–195. [CrossRef]
3. Tanase, S.; Reedijk, J. Chemistry and magnetism of cyanido-bridged d–f assemblies. *Coord. Chem. Rev.* **2006**, *250*, 2501–2510. [CrossRef]
4. Ohkoshi, S.-I.; Tokoro, H. Photomagnetism in Cyano-Bridged Bimetal Assemblies. *Accounts Chem. Res.* **2012**, *45*, 1749–1758. [CrossRef] [PubMed]
5. Pal, S.; Dey, K.; Benmansour, S.; Gómez-García, C.J.; Nayek, H.P. Syntheses, structures and magnetic properties of cyano-bridged one-dimensional Ln^{3+} – Fe^{3+} (Ln = La, Dy, Ho and Yb) coordination polymers. *New J. Chem.* **2019**, *43*, 6228. [CrossRef]

6. Rebilly, J.-N.; Catala, L.; Rivière, E.; Guillot, R.; Wernsdorfer, W.; Mallah, T. One step assembly of a nonanuclear Cuii2Niii7 bimetallic cyanide bridged complex. *Chem. Commun.* **2006**, 735–737. [\[CrossRef\]](#)
7. Ferbinteanu, M.; Kajiwaru, T.; Choi, K.-Y.; Nojiri, H.; Nakamoto, A.; Kojima, N.; Cimpoesu, F.; Fujimura, Y.; Takaishi, S.; Yamashita, M. A binuclear Fe(III)Dy(III) single molecule magnet. Quantum Effects and Models. *J. Am. Chem. Soc.* **2006**, *128*, 9008. [\[CrossRef\]](#)
8. Sun, O.; Chen, P.; Li, H.-F.; Gao, T.; Yan, P.-F. Wheel-like {Ln6} luminescent lanthanide complexes covering the visible and near-infrared domains. *CrystEngComm* **2020**, *22*, 5200. [\[CrossRef\]](#)
9. Wang, R.; Wang, H.; Wang, J.; Bai, F.; Ma, Y.; Li, L.; Wang, Q.; Zhao, B.; Cheng, P. The different magnetic relaxation behaviors in [Fe(CN)6]3− or [Co(CN)6]3− bridged 3d–4f heterometallic compounds. *CrystEngComm* **2020**, *22*, 2998. [\[CrossRef\]](#)
10. Petiot, L.; Cabral, F.M.; Formiga, A.L.; Mazali, I.O.; Sigoli, F.A. A series of three isostructural 1D lanthanide coordination network based on 4,4',4''-(benzene-1,3,5-triyltris(methylene))tris(oxy)tribenzoate ligand: Synthesis, crystal structure and photophysical properties. *Inorg. Chim. Acta* **2019**, *494*, 21–29. [\[CrossRef\]](#)
11. Chen, W.-B.; Zhong, L.; Zhong, Y.-J.; Zhang, Y.-Q.; Gao, S.; Dong, W. Understanding the near-infrared fluorescence and field-induced single-molecule-magnetic properties of dinuclear and one-dimensional-chain ytterbium complexes based on 2-hydroxy-3-methoxybenzoic acid. *Inorg. Chem. Front.* **2020**, *7*, 3136–3145. [\[CrossRef\]](#)
12. Chorazy, S.; Rams, M.; Nakabayashi, K.; Sieklucka, B.; Ohkoshi, S.-i. White light emissive dyiii single-molecule magnets sensitized by diamagnetic [CoIII(CN)6]3− linkers. *Chem. Eur. J.* **2016**, *22*, 7371. [\[CrossRef\]](#)
13. Barry, D.E.; Caffrey, D.F.; Gunnlaugsson, T. Lanthanide-directed synthesis of luminescent self-assembly supramolecular structures and mechanically bonded systems from acyclic coordinating organic ligands. *Chem. Soc. Rev.* **2016**, *45*, 3244. [\[CrossRef\]](#)
14. Li, J.-R.; Chen, W.-T.; Tong, M.-L.; Guo, G.-C.; Tao, Y.; Yu, Q.; Song, W.-C.; Bu, X.-H. Cyano-Bridged LnIII–FeIII Complexes with Alternative Monosulfoxides as Blocking Ligands. *Cryst. Growth Des.* **2008**, *8*, 2780–2792. [\[CrossRef\]](#)
15. Wilson, D.C.; Liu, S.; Chen, X.; Meyers, E.A.; Bao, X.; Prosvirnin, A.V.; Dunbar, K.R.; Hadad, C.M.; Shore, S.G. Water-free rare earth-prussian blue type analogues: Synthesis, structure, computational analysis, and magnetic data of {LnIII(DMF)6FeIII(CN)6}∞ (Ln = Rare Earths Excluding Pm). *Inorg. Chem.* **2009**, *48*, 5725. [\[CrossRef\]](#)
16. Akitsu, T.; Einaga, Y. Structures and XPS studies of several 3d–4f cyano-bridged LnIII–FeIII/CoIII heterometallic complexes. *Polyhedron* **2006**, *25*, 2655–2662. [\[CrossRef\]](#)
17. Qian, S.-Y.; Zhou, H.; Yuan, A.-H.; Song, Y. Syntheses, structures, and magnetic properties of five novel octacyano-metallate-based lanthanide complexes with helical chains. *Cryst. Growth Des.* **2011**, *11*, 5676. [\[CrossRef\]](#)
18. Chorazy, S.; Wyczesany, M.; Sieklucka, B. Lanthanide photoluminescence in heterometallic polycyanidometal-late-based coordination networks. *Molecules* **2017**, *22*, 1902. [\[CrossRef\]](#)
19. Long, J.; Chamoiseau, L.-M.; Mathonière, C.; Marvaud, V. Photoswitchable heterotrimetallic chain based on octacyano-anomolybdate, copper, and nickel: Synthesis, characterization, and photomagnetic properties. *Inorg. Chem.* **2009**, *48*, 22. [\[CrossRef\]](#)
20. Koner, R.; Drew, M.G.B.; Figuerola, A.; Diaz, C.; Mohanta, S. A new cyano-bridged one-dimensional GdIII/FeIII co-ordination polymer with o-phenanthroline as the blocking ligand: Synthesis, structure, and magnetic properties. *Inorg. Chim. Acta* **2005**, *358*, 3041. [\[CrossRef\]](#)
21. Zhang, R.-F.; Zhao, B.; Wang, H.-S.; Cheng, P. Two novel 2-D homometallic cyano-bridged complexes: Synthesis, structures and fluorescent properties. *Inorg. Chem. Commun.* **2007**, *10*, 1226–1228. [\[CrossRef\]](#)
22. Liu, Y.; Chen, Y.-C.; Liu, J.; Chen, W.-B.; Huang, G.-Z.; Wu, S.-G.; Wang, J.; Liu, J.-L.; Tong, M.-L. Cyanometal-late-bridged didysprosium single-molecule magnets constructed with single-ion magnet building Block. *Inorg. Chem.* **2020**, *59*, 687. [\[CrossRef\]](#) [\[PubMed\]](#)
23. Hulliger, F.; Landolt, M.; Vetsch, H. Rare-earth ferricyanides and chromicyanides LnT(CN)6·nH2O. *J. Solid State Chem.* **1976**, *18*, 283. [\[CrossRef\]](#)
24. Chorazy, S.; Zychowicz, M.; Ohkoshi, S.-i.; Sieklucka, B. Wide-range UV-to-visible excitation of near-infrared emission and slow magnetic relaxation in LnIII(4,4'-Azopyridine-1,1'-dioxide)[CoIII(CN)6]3− layered frameworks. *Inorg. Chem.* **2019**, *58*, 165. [\[CrossRef\]](#)
25. Binnemans, K.; Van Deun, R.; Görlner-Walrand, C.; Adam, J.L. Spectroscopic properties of trivalent lanthanide ions in fluorophosphate glasses. *J. Non-Cryst. Solids* **1998**, *238*, 11. [\[CrossRef\]](#)
26. Figuerola, A.; Ribas, J.; Llunell, M.; Casanova, D.; Maestro, M.; Alvarez, S.; Diaz, C. Magnetic properties of cyano-bridged Ln3+–M3+ complexes. Part I: Trinuclear complexes (Ln3+ = La, Ce, Pr, Nd, Sm; M3+ = FeLS, Co) with bpy as blocking ligand. *Inorg. Chem.* **2005**, *44*, 6939. [\[CrossRef\]](#)
27. Alexandru, M.-G.; Visinescu, D.; Shova, S.; Lloret, F.; Julve, M.; Andruh, M. Two-dimensional coordination polymers constructed by [NiIIILnIII] nodes and [WIV(bpy)(CN)6]2− spacers: A network of [NiIIDyIII] single molecule magnets. *Inorg. Chem.* **2013**, *52*, 11627. [\[CrossRef\]](#)
28. Li, G.; Yan, P.; Sato, O.; Einaga, Y. The structure, photo-induced magnetization and correlation of the cyano-bridged two-dimensional hetero-bimetallic compounds. *J. Solid State Chem.* **2005**, *178*, 36–40. [\[CrossRef\]](#)
29. Burns, C.P.; Yang, X.; Sung, S.; Wofford, J.D.; Bhuvanesh, N.S.; Hall, M.B.; Nippe, M. Towards understanding of lanthanide-transition metal bonding: Investigations of the first Ce–Fe bonded complex. *Chem. Commun.* **2018**, *54*, 10893–10896. [\[CrossRef\]](#)
30. Muddassir, M. Syntheses, structural characterization, and thermal behavior of cyanide-bridged [2 + 2]-type tetranuclear rectangle-based molecule constructed from Tm(III) and hexacyanocobaltate(III). *Transit. Met. Chem.* **2020**, *45*, 317. [\[CrossRef\]](#)

31. Muddassir, M. A new 1D Cu(II)-W(Cn)₈ based coordination polymer: Crystallographic structural architecture, Hirshfeld surface, DFT and luminescent analyses. *J. Organomet. Chem.* **2020**, *926*, 121499. [\[CrossRef\]](#)
32. Muddassir, M.; Alarifi, A.; Afzal, M. Synthesis, structural topology, DFT, and photoluminescence properties of Sm(III) and octacyanomolybdate(V) building-block-based 1-D chain complex. *Transit. Met. Chem.* **2020**, *46*, 129–137. [\[CrossRef\]](#)
33. Muddassir, M.; Alarifi, A.; Afzal, M.; Sepay, N. Newly designed Mn(III)–W(V) bimetallic assembly built by manganese(III) Schiff-base and octacyanotungstate(V) building blocks: Structural topologies, and magnetic features. *Appl. Organomet. Chem.* **2020**, *34*, e5914. [\[CrossRef\]](#)
34. Casanova, D.; Llunell, M.; Alemany, P.; Alvarez, S. The Rich Stereochemistry of Eight-Vertex Polyhedra: A Continuous Shape Measures Study. *Chem.—A Eur. J.* **2005**, *11*, 1479–1494. [\[CrossRef\]](#)
35. Alexandrov, E.V.; Blatov, V.A.; Kochetkov, A.V.; Proserpio, D.M. Underlying nets in three-periodic coordination polymers: Topology, taxonomy and prediction from a computer-aided analysis of the Cambridge Structural Database. *CrystEngComm* **2011**, *13*, 3947–3958. [\[CrossRef\]](#)
36. Wu, L.-C.; Nielsen, M.B.; Bremholm, M.; Madsen, S.R.; Overgaard, J.; Newville, M.; Chen, Y.-S.; Iversen, B.B. High pressure induced charge transfer in 3d–4f bimetallic photomagnetic materials. *Chem. Commun.* **2015**, *51*, 8868–8871. [\[CrossRef\]](#)
37. Sánchez-Moreno, M.; Choquesillo-Lazarte, D.; González-Pérez, J.; Carballo, R.; Castiñeiras, A.; Niclós-Gutiérrez, J. Inter-ligand interactions and the selective formation of the unusual metal–N₃(adenine) bond in ternary copper(II) complexes with N-benzyliminodiacetato(2–) ligands. *Inorg. Chem. Commun.* **2002**, *5*, 800–802. [\[CrossRef\]](#)
38. Lin, Q.-H.; Li, Y.-C.; Qi, C.; Liu, W.; Wang, Y.; Pang, S.-P. Nitrogen-rich salts based on 5-hydrazino-1H-tetrazole: A new family of high-density energetic materials. *J. Mater. Chem. A* **2013**, *1*, 6776–6785. [\[CrossRef\]](#)
39. Song, X.-J.; Muddassir, M.; Chen, Y.; Wang, H.-S.; Song, Y.; You, X.-Z. Magnetic properties of two 2D complexes based on 1D chain containing [Fe(bpy)(CN)₄][–] unit. *Dalton Trans.* **2013**, *42*, 1116. [\[CrossRef\]](#)
40. Choi, H.J.; Sokol, J.J.; Long, J.R. High-spin metal–cyanide clusters: Species incorporating [Mn(salen)]⁺ complexes as a source of anisotropy. *J. Phys. Chem. Solids* **2003**, *65*, 839–844. [\[CrossRef\]](#)
41. McKinnon, J.J.; Fabbiani, F.P.A.; Spackman, M.A. Comparison of Polymorphic Molecular Crystal Structures through Hirshfeld Surface Analysis. *Cryst. Growth Des.* **2007**, *7*, 755–769. [\[CrossRef\]](#)
42. Spackman, M.A.; Jayatilaka, D. Hirshfeld surface analysis. *CrystEngComm* **2009**, *11*, 19. [\[CrossRef\]](#)
43. Mahmoudi, G.; Castiñeiras, A.; Garczarek, P.; Bauzá, A.; Rheingold, A.L.; Kinzhybalo, V.; Frontera, A. Synthesis, X-ray characterization, DFT calculations and Hirshfeld surface analysis of thiosemicarbazone complexes of Mn⁺ ions (n = 2, 3; M = Ni, Cd, Mn, Co and Cu). *CrystEngComm* **2016**, *18*, 1009. [\[CrossRef\]](#)
44. SeethaLekshmi, S.; Ramya, A.; Reddy, M.; Varughese, S. Lanthanide complex-derived white-light emitting solids: A survey on design strategies. *J. Photochem. Photobiol. C Photochem. Rev.* **2017**, *33*, 109–131. [\[CrossRef\]](#)
45. Carter, K.P.; Zulato, C.H.F.; Cahill, C.L. Exploring supramolecular assembly and luminescent behavior in a series of RE-p-chlorobenzoic acid-1,10-phenanthroline complexes. *CrystEngComm* **2014**, *16*, 10189–10202. [\[CrossRef\]](#)
46. Bünzli, J.-C.G. On the design of highly luminescent lanthanide complexes. *Coord. Chem. Rev.* **2015**, *293–294*, 19–47. [\[CrossRef\]](#)
47. Zhang, A.; Zhang, J.; Pan, Q.; Wang, S.; Jia, H.; Xu, B. Synthesis, photoluminescence and intramolecular energy transfer model of a dysprosium complex. *J. Lumin.* **2012**, *132*, 965–971. [\[CrossRef\]](#)